DOI: 10.19884/j.1672-5220.202403015

Magnetic Resonance Image Super-Resolution Based on GAN and Multi-Scale Residual Dense Attention Network

GUAN Chunling, YU Suping*, XU Wujun, FAN Hong
College of Information Science and Technology, Donghua University, Shanghai 201620, China

Abstract: The application of image super-resolution (SR) has brought significant assistance in the medical field, aiding doctors to make more precise diagnoses. However, solely relying on a convolutional neural network (CNN) for image SR may lead to issues such as blurry details and excessive smoothness. To address the limitations, we proposed an algorithm based on the generative adversarial network (GAN) framework. In the generator network, three different sizes of convolutions connected by a residual dense structure were used to extract detailed features, and an attention mechanism combined with dual channel and spatial information was applied to concentrate the computing power on crucial areas. In the discriminator network, using InstanceNorm to normalize tensors sped up the training process while retaining feature information. The experimental results demonstrate that our algorithm achieves higher peak signal-to-noise ratio (PSNR) and structural similarity index measure (SSIM) compared to other methods, resulting in an improved visual quality.

Keywords: magnetic resonance (MR); image super-resolution (SR); attention mechanism; generative adversarial network (GAN); multi-scale convolution
CLC number: TP317.4 **Document code**: A
Article ID: 1672-5220(2025)04-0435-07

Open Science Identity (OSID)

0 Introduction

Medical imaging plays an important role in medical diagnoses. Magnetic resonance (MR) imaging utilizes a strong magnetic field to magnetize water molecules in the human body and capture signals, particularly prominent in areas with high water content. In the meantime, it is non-radioactive and does not cause any harm to the human body.

High-resolution (HR) MR images contain rich details. They provide detailed anatomical information, improve the accuracy of medical diagnosis, and greatly assist in subsequent medical treatments. However, obtaining them is a challenge, typically with longer scanning time required and spatial coverage limited. If we can get super-resolution (SR) images from low-resolution (LR) images, we can obtain higher-quality images at a lower cost. To improve the resolution of MR images, it is necessary to study the degradation process of MR images and find the relationship between HR and their corresponding LR. As shown in Fig. 1, besides down-sampling, the factors that may cause resolution reduction are other magnetic field interference, patient movement, poor performance of the MR machine and transmission noise.

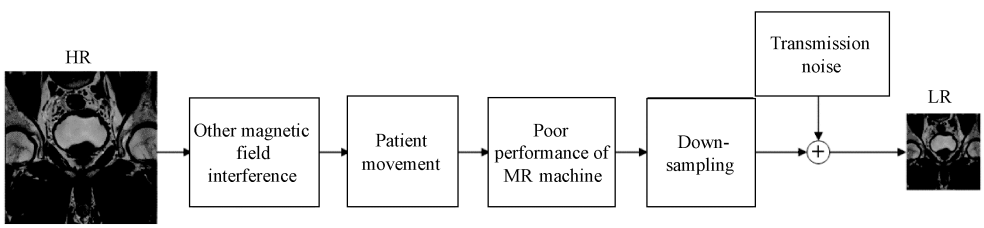

Fig. 1 Degradation process of MR image

1 Related Work

Image SR methods can be categorized into interpolation, reconstruction and deep learning[1]. Deep learning holds great potential in image processing and medical diagnoses.

The convolutional neural network (CNN) is a feedforward neural network that can respond to the surrounding units within a certain receptive field, making

Received date: 2024-03-28
* Correspondence should be addressed to YU Suping, email: yusuping@dhu.edu.cn
Citation: GUAN C L, YU S P, XU W J, et al. Magnetic resonance image super-resolution based on GAN and multi-scale residual dense attention network[J]. *Journal of Donghua University (English Edition)*, 2025, 42(4): 435-441.

it particularly effective for processing large images. Therefore, CNN has been widely used in various computer vision tasks, including SR. The methods based on deep learning are accustomed to employing CNN to extract texture from images, such as the SR by CNN (SRCNN)[2] and the enhanced deep residual networks for SR (EDSR)[3].

The generative adversarial network (GAN)[4] is an architecture proposed by Goodfellow. Ledig et al.[5] introduced the GAN framework into the field of SR and proposed SRGAN, which utilized the residual network (ResNet)[6] as the generator network. Compared to the SR images generated solely by CNN, the SR images generated by SRGAN exhibit clear textures, aligning more with human visual perception.

Due to the significant advantages of CNN and GAN in image processing, computer vision techniques have been widely employed to assist in the diagnosis from medical images. Xi et al.[7] proposed a medical image SR algorithm based on ResNet for continuous two-dimensional slices of MR images. Chen et al.[8] introduced an SR model for medical images based on the principles of recursive neural networks. Ankitha et al.[9] used a GAN-based network with residual blocks to extract features for brain MR images. Iwamoto et al.[10] applied the idea of enhancing LR T2-weighted images using HR T1-weighted images. Lin et al.[11] proposed a novel slice-profile transformation-based SR framework with deep generative learning to reconstruct three-dimensional MR images. These advancements illustrate the critical role of CNNs and GANs in pushing the boundaries of medical image SR.

2 Methods

MR image quality evaluation should consider not only objective assessment metrics but also assistance in medical diagnoses and treatments. The image structure and the abnormal texture can seriously affect the result of the diagnosis.

The texture details are significant, yet most of the images reconstructed based on CNN are often excessively smooth. Therefore, we propose an algorithm based on GAN and a multi-scale residual dense attention network.

2.1 Architecture of network

The main architecture of our algorithm is based on GAN. The network consists of two parts: the generator and the discriminator (Fig. 2). The generator is composed of shallow feature extraction, deep feature extraction and reconstruction. The deep feature extraction network consists of multi-scale residual dense attention blocks (MRDABs), which are composed of multi-scale residual dense blocks (MSRDBs) and dual parallel attention modules (DPAMs), as shown in Fig. 2(a).

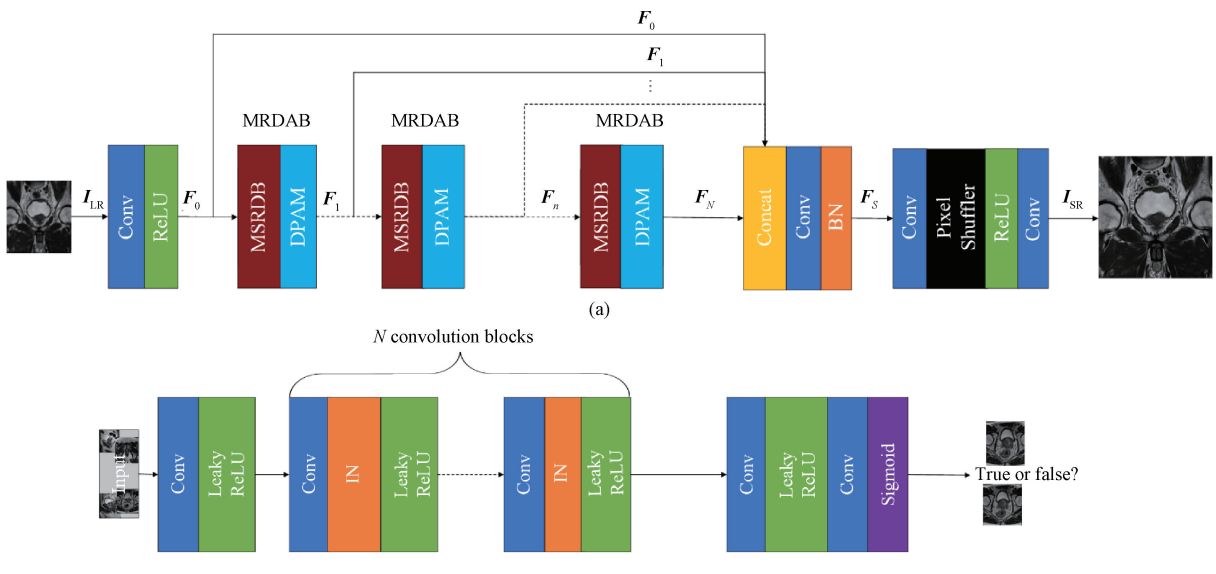

Conv—convolution operation; Concat—concatenate; BN—batch normalization; IN—instance normalization.

Fig. 2 Architecture of our algorithm: (a) generator; (b) discriminator

The LR image $\boldsymbol{I}_{\mathrm{LR}}$ is processed through a 3×3 convolutional layer with a rectified linear unit (ReLU) activation function for shallow feature extraction. $\boldsymbol{F}_0$ is the shallow feature map, $\mathrm{Conv}_{3\times3}(\cdot)$ is a convolution operation with a kernel size of 3×3 and the formula is

$$\boldsymbol{F}_0 = \mathrm{Conv}_{3\times3}(\boldsymbol{I}_{\mathrm{LR}}). \tag{1}$$

In this step, the three channels of $\boldsymbol{I}_{\mathrm{LR}}$ are extended to 64 channels of $\boldsymbol{F}_0$, facilitating subsequent feature extraction. After shallow feature extraction, the extracted feature maps are then input into the deep feature extraction network. The MRDAB uses residual dense connections to concatenate the feature maps $\boldsymbol{F}_n$, $n = 1, 2, \cdots, N$. The formulas of the network and combination are

$$\boldsymbol{F}_n = \mathrm{MRDAB}(\boldsymbol{F}_{n-1}), \tag{2}$$

$$\boldsymbol{F}_S = \mathrm{Concat}(\boldsymbol{F}_0, \boldsymbol{F}_1, \cdots, \boldsymbol{F}_N), \quad (3)$$

where Concat, i. e., concatenate, is a method of characteristic fusion, and the feature maps obtained from the previous convolution block are combined and calculated by the convolution layer to get $\boldsymbol{F}_S$.

At the last step of the network, the SR image $\boldsymbol{I}_{SR}$ is obtained by the sub-pixel convolution UPscale. It can be expressed as

$$\boldsymbol{I}_{SR} = \mathrm{UPscale}(\boldsymbol{F}_S). \quad (4)$$

As shown in Fig. 2(b), the discriminator is mainly composed of convolutional blocks which contain convolution, normalization (BN and IN) and activation function (Leaky ReLU). At last, the probability of the input image being real is output.

2.2 Architecture of MSRDB

The MSRDB is utilized to capture complex feature information from MR images. As shown in Fig. 3, this block combines the multi-scale convolution groups (MSCGs) and residual dense connection, employing multiple convolution kernels of different sizes to extract structural and detailed features, enhancing the texture of SR images, and the set of formulas of the convolution is

$$\begin{cases} \boldsymbol{H}_{i,1} = \mathrm{Conv}_{3\times3}(\boldsymbol{G}_i), \\ \boldsymbol{H}_{i,2} = \mathrm{Conv}_{5\times5}(\boldsymbol{G}_i), \\ \boldsymbol{H}_{i,3} = \mathrm{Conv}_{7\times7}(\boldsymbol{G}_i), \end{cases} \quad (5)$$

where the input feature map $\boldsymbol{G}_i$ is divided into three tensors as $\boldsymbol{H}_{i,1}$, $\boldsymbol{H}_{i,2}$, $\boldsymbol{H}_{i,3}$ ($i = 1, 2, \cdots, N$); i represents the i-layer MSCG in MSRDB.

The dense connections transfer the extracted feature maps from each layer to the subsequent layer, thereby preserving feature and gradient information, and preventing model collapse[12]. In Fig. 4, each layer of the convolution group uses convolutions with kernel sizes of 3×3, 5×5 and 7×7 to provide different sizes of receptive fields for the network. The detailed features are extracted at a small scale, such as 3×3 and 5×5 convolutions. The receptive field of a 7×7 convolution is capable of extracting the structural features of the target[13]. The ReLU activation function is applied to the results, and the channel number is transformed from 64 to 16. Subsequently, the input $\boldsymbol{G}_i$ and the results of each convolutional layer $\boldsymbol{H}_{i,1}$, $\boldsymbol{H}_{i,2}$, $\boldsymbol{H}_{i,3}$ are concatenated as $\boldsymbol{G}_{i+1}$ ($i = 1, 2, \cdots, N$) and fed into the next convolution group, with the number of feature channels c transformed from c to $c+16 \times 3$. The formula of the combination is

$$\boldsymbol{G}_{i+1} = \mathrm{Concat}(\boldsymbol{H}_{i,2}, \boldsymbol{H}_{i,2}, \boldsymbol{H}_{i,3}, \boldsymbol{G}_i). \quad (6)$$

As shown in Fig. 3, after repeating this process for convolution groups, the output feature map contains the processed feature maps from each layer, preserving the texture information of the image to a great extent[14].

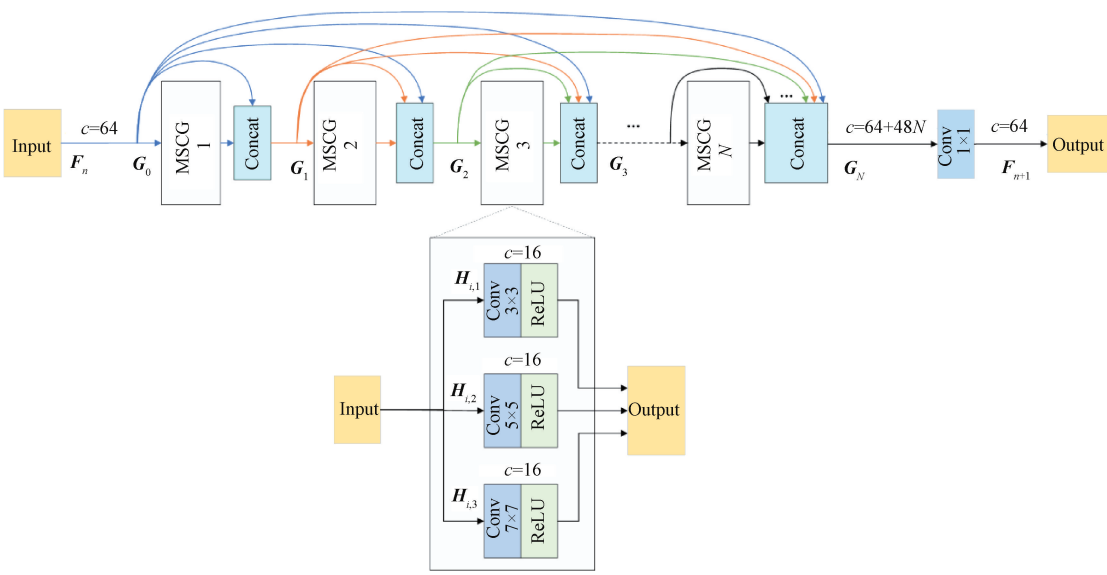

Fig. 3 Architecture of MSRDB

2.3 Contents of DPAM

After shallow feature extraction, each part of the feature maps carries equal weight. By adding attention mechanisms, the model can focus on the regions which have important features[15-16].

In this study, two different types of attention mechanisms are used in parallel to weigh different regions. As shown in Fig. 4, the output $\boldsymbol{F}_{n-1}$ of MSRDB is fed into the spatial attention mechanism (SAM) and parallel channel attention mechanism (PCAM) to get the weights k_1 and k_2, then they multiply with $\boldsymbol{F}_{n-1}$ to get $\boldsymbol{A}_1$ and $\boldsymbol{A}_2$. The sum $\boldsymbol{F}_n$ of $\boldsymbol{A}_1$, $\boldsymbol{A}_2$ and $\boldsymbol{F}_{n-1}$ is the input of the next MSRDB.

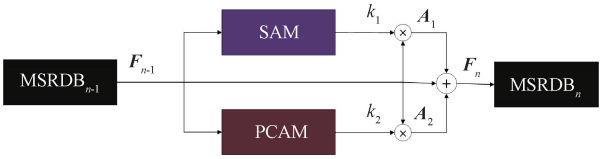

Fig. 4 Contents of DPAM

2.3.1 Contents of SAM

The contents of SAM are shown in Fig. 5. $\boldsymbol{F}_{n-1}$ is used as the input of SAM. $\boldsymbol{P}_1$ and $\boldsymbol{P}_2$ are respectively obtained by max pooling (MaxPool) and average pooling (AvgPool). These two feature maps are then concatenated to obtain the complete feature map $\boldsymbol{P}$, and the formulas of the feature maps are

$$\begin{cases} \boldsymbol{P}_1 = \text{MaxPool}(\boldsymbol{F}_{n-1}), \\ \boldsymbol{P}_2 = \text{AvgPool}(\boldsymbol{F}_{n-1}), \end{cases} \tag{7}$$

$$\boldsymbol{P} = \text{Concat}(\boldsymbol{P}_1, \boldsymbol{P}_2). \tag{8}$$

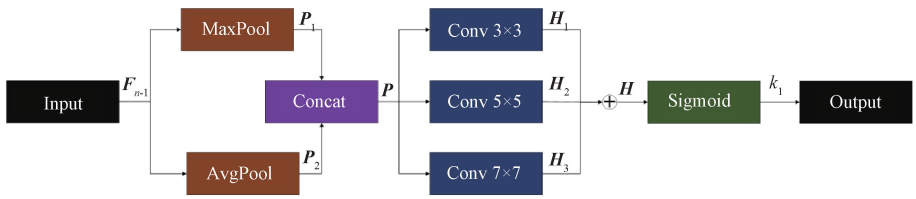

Fig. 5 Contents of SAM

In SAM, a larger receptive field enhances the global information extraction capability. Therefore, an improved SAM is used, which uses 3 × 3, 5 × 5 and 7 × 7 convolutional kernels to capture the importance of spatial positions. The set of formulas can be expressed as

$$\begin{cases} \boldsymbol{H}_1 = \text{Conv}_{3\times3}(\boldsymbol{P}), \\ \boldsymbol{H}_2 = \text{Conv}_{5\times5}(\boldsymbol{P}), \\ \boldsymbol{H}_3 = \text{Conv}_{7\times7}(\boldsymbol{P}). \end{cases} \tag{9}$$

The feature maps $\boldsymbol{H}_1$, $\boldsymbol{H}_2$ and $\boldsymbol{H}_3$ are fused by adding the corresponding positions, and finally, a sigmoid activation function σ is applied to generate the spatial attention feature map $\boldsymbol{H}$ with weight k_1 and the formulas are

$$\boldsymbol{H} = \boldsymbol{H}_1 \oplus \boldsymbol{H}_2 \oplus \boldsymbol{H}_3, \tag{10}$$

$$k_1 = \sigma(\boldsymbol{H}). \tag{11}$$

2.3.2 Contents of PCAM

PCAM is based on the squeeze and excitation (SE) attention mechanism. Figure 6 shows the contents of PCAM. $\boldsymbol{F}_{n-1}$ is used as the input of PCAM. The size of the input $\boldsymbol{F}_{n-1}$ is $h \times w \times c$, the variables h and w represent the height and width of $\boldsymbol{F}_{n-1}$, c denotes the number of channels. Then $\boldsymbol{F}_{n-1}$ is transformed by average pooling into three tensors with different sizes: $\boldsymbol{P}_1(1, 1, c)$, $\boldsymbol{P}_2(2, 2, c)$ and $\boldsymbol{P}_4(4, 4, c)$. The set of formulas is

$$\begin{cases} \boldsymbol{P}_1 = \text{AvgPool}_1(\boldsymbol{F}_{n-1}), \\ \boldsymbol{P}_2 = \text{AvgPool}_2(\boldsymbol{F}_{n-1}), \\ \boldsymbol{P}_4 = \text{AvgPool}_4(\boldsymbol{F}_{n-1}). \end{cases} \tag{12}$$

The tensors are resized and concatenated into a tensor $\boldsymbol{P}'$. The squeezing process is completed and the formula is

$$\boldsymbol{P}' = \text{Concat}(\boldsymbol{P}_1, \boldsymbol{P}_2, \boldsymbol{P}_4). \tag{13}$$

The tensor is passed through two fully connected layers to capture complex correlations between channels, resulting in a channel attention feature map with the weight k_2. The corresponding function is defined as FC(·), and the formula is

$$k_2 = \text{FC}(\boldsymbol{P}'). \tag{14}$$

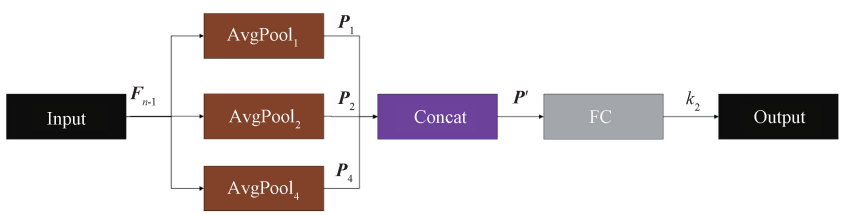

Fig. 6 Contents of PCAM

3 Experiments

3.1 Dataset

The MR images are obtained from the PROSTATEx and PROSTATE-DIAGNOSIS datasets of the Cancer Imaging Archive. Images are randomly split into an 8∶1∶1 ratio, as 2 000 images for training, 250 images for validation and 250 images for testing.

3.2 Experimental environment and setting

The experimental environment used NVIDIA GeForce RTX 3080Ti GPU, Python 3.8, PyTorch 1.11, Ubuntu18.04, CUDA 11.3 and torchvision 0.12.0. During the training process, the adaptive moment

estimation (Adam) was used as the optimizer, the batch size was 32, the learning rate was 0.000 1, and the feature extraction block number was 8.

3.3 Ablation experiment

To verify the performance of each module in the algorithm, the residual blocks, residual dense blocks and MSRDBs are subjected to an ablation experiment at a scale factor of 4. The GAN is used as the framework, and different modules are integrated into the generator for deep feature extraction.

Objective evaluation metrics include peak signal-to-noise ratio (PSNR) and structural similarity index measure (SSIM). PSNR indicates the level of image distortion, with higher values corresponding to better reconstruction quality. SSIM mainly evaluates the similarity between images. The closer the value is to 1, the closer the reconstructed image is to the original image.

The result of the experiment is shown in Table 1, demonstrating that dense connections enhance the information utilization efficiency of the network. Additionally, the multi-scale convolution kernels can extract richer feature texture information, and the larger size convolution kernel extraction can improve PSNR. A PSNR of 26.739 3 dB and an SSIM of 0.739 7 are achieved by using a set of kernel sizes (3×3, 5×5 and 7×7) in a multi-scale convolution. Therefore, the kernel size combination of 3×3, 5×5 and 7×7 is chosen in the algorithm.

Table 1 Experimental parameters of different kernel sizes and connections

Kernel size	Connection	Epoch	PSNR/dB	SSIM
3×3	Residual	200	26.343 4	0.726 7
3×3	Residual dense	200	26.409 2	0.734 1
3×3 and 5×5	Residual dense	200	26.621 3	0.737 7
1×1, 3×3 and 5×5	Residual dense	200	26.633 6	0.737 0
3×3, 5×5 and 7×7	Residual dense	200	26.739 3	0.739 7

Using MSRDB as the baseline, we conducted additional ablation experiments by adding SAM, PCAM and DPAM, respectively. As shown in Table 2, when the training epochs are 200, compared with no attention mechanism, PCAM gets the SSIM higher, and DPAM gets the PSNR higher.

Table 2 Attention mechanism experimental results

Method	PSNR/dB	SSIM
No attention mechanism	26.739 3	0.739 7
SAM	26.778 5	0.740 2
PCAM	26.774 2	**0.740 3**
DPAM	**26.804 4**	0.740 0

3.4 Comparison with other algorithms

The proposed algorithm is tested with representative SR networks such as the classical algorithms Bicubic, SRCNN, Fast SRCNN (FSRCNN), EDSR and SRGAN. The image quality data of the comparison experiment is shown in Table 3. Our algorithm achieves superior PSNR and SSIM compared with other algorithms. The number of parameters and the test time of the algorithms in the comparison experiment are shown in Table 4. Our algorithm has 1.84×10^7 parameters, and its test time is 107 s for 250 images. Compared with other neural networks, our algorithm requires more time and parameters, but PSNR and SSIM are improved. Compared with SRGAN, our algorithm requires only 3% more time but achieves significant quality improvements: PSNR increases by approximately 2.4 dB at scale factors of both 4 and 2; SSIM improves by 0.027 6 and 0.009 8 at scale factors of 4 and 2, respectively.

Table 3 Objective data of comparison experiment at scale factors of 4 and 2

Algorithm	PSNR/dB		SSIM	
	× 4	× 2	× 4	× 2
Bicubic	23.669 5	27.922 0	0.603 2	0.817 3
SRCNN	26.003 5	31.825 2	0.727 5	0.910 7
FSRCNN	26.105 2	31.563 0	0.727 6	0.906 9
EDSR	27.417 3	33.054 9	0.764 9	0.913 5
SRGAN	25.044 9	30.852 3	0.738 7	0.907 5
Ours	27.460 9	33.293 8	0.766 3	0.917 3

Note: × 4 and × 2 denote at the scale factors of 2 and 4, respectively.

Table 4 Time efficiency data of comparison experiment

Algorithm	Number of parameters	Test time/s
Bicubic	—	76
SRCNN	5.6×10^4	93
FSRCNN	1.4×10^4	83
EDSR	9.41×10^5	81
SRGAN	6.2×10^6	103
Ours	1.84×10^7	107

Note: — denotes that the Bicubic algorithm does not need the training step.

As shown in Fig. 7(a), when the scale factor is 4, the effect of Bicubic interpolation is the most blurred, while SRCNN and FSRCNN recover some details but also blur the texture. The PSNR and SSIM of EDSR are higher (Table 3), but its edges are smooth, and small

details are not restored. While SRGAN offers clear visual effects, it suffers from square block artifacts that can hinder medical diagnosis. Compared to the mentioned algorithms, our algorithm can restore more image details, especially in areas such as blood vessels, making it suitable for MR images with minimal disease.

When the scale factor is 2, the results are shown in Fig. 7 (b). The effects of SRCNN and FSRCNN are poor. The SR images from other algorithms show small visual differences to the human eye, but the artifacts affecting small details such as blood vessels in the SRGAN algorithm are more obvious, and its image graininess is more pronounced. Our algorithm also achieves good visual results.

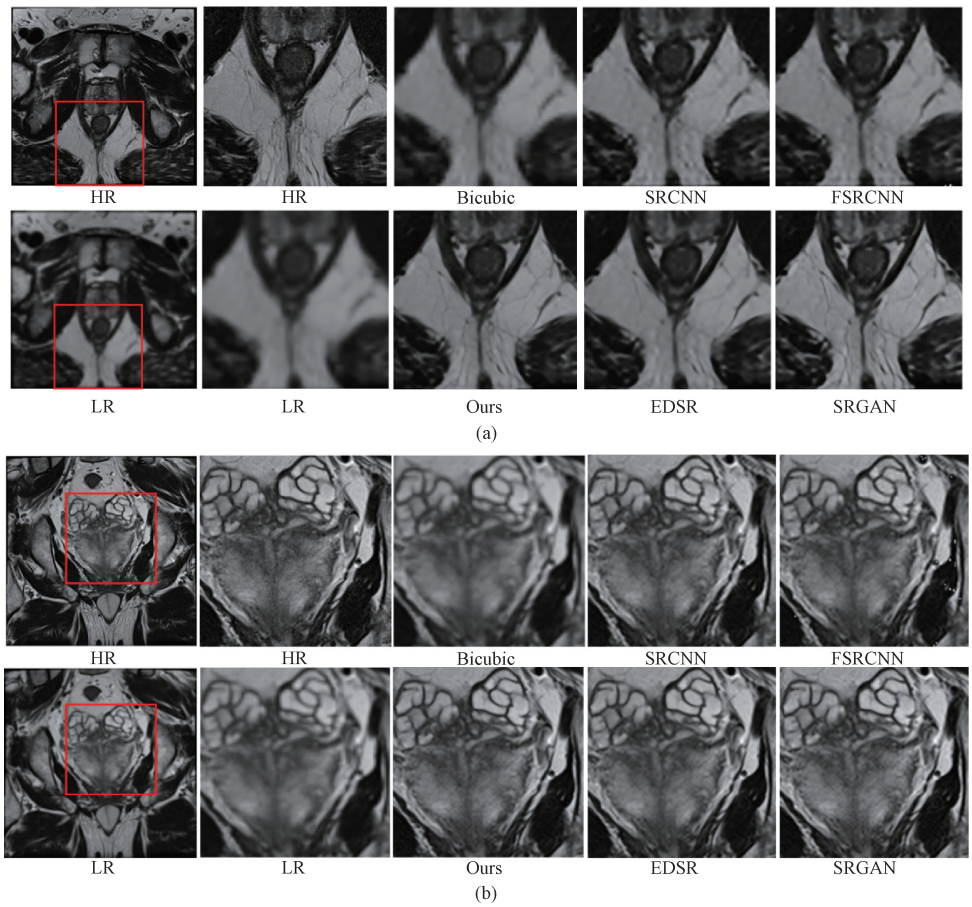

Fig. 7 Reconstruction results of red region by different algorithms at different scale factors: (a) 4; (b) 2

4 Conclusions

Based on CNN and GAN, we use deep learning technology to study image SR and its application in MR. Aiming at the special properties of MR images, the algorithm based on the GAN framework is proposed for SR images. Although this algorithm consumes more computing resources, it achieves higher PSNR and SSIM compared to other methods, resulting in an improved visual quality. At a scale factor of 2, the algorithm achieves a PSNR of 33.293 8 dB and an SSIM of 0.917 3. Correspondingly, at a scale factor of 4, the PSNR is measured at 27.460 9 dB, with an SSIM of 0.766 3. Additionally, the improvement in visual perception is more pronounced at the scale factor of 4.

In the follow-up work, we plan to use dilated convolution or deep separable convolution to reduce the number of parameters of the network and decrease its occupancy of computing resources.

References

[1] TANG Y Q, PAN H, ZHU Y P. A survey of super resolution image reconstruction [J]. *Journal of Electronics*, 2020, 48 (7): 1407-1420. (in Chinese)

[2] DONG C, LOY C C, HE K M, et al. Image super-resolution using deep convolutional networks [J]. *IEEE Transactions on Pattern Analysis and Machine Intelligence*, 2016, 38 (2): 295-307.

[3] LIM B, SON S, KIM H, et al. Enhanced deep residual networks for single image super-resolution [C]//Proceedings of the IEEE Conference on Computer Vision and Pattern Recognition. New York: IEEE, 2017: 136-144.

[4] GOODFELLOW I J, POUGHT-ABADIE J, MIRZA

M, et al. Generative adversarial nets [C]// Advances in Neural Information Processing Systems. Cambridge: MIT Press, 2014: 2672-2680.
[5] LEDIG C, THEIS L, HUSZÁR F, et al. Photo-realistic single image super-resolution using a generative adversarial network [C]//2017 IEEE Conference on Computer Vision and Pattern Recognition (CVPR). New York: IEEE, 2017: 105-114.
[6] HE K M, ZHANG X Y, REN S Q, et al. Deep residual learning for image recognition [C]// Proceedings of the IEEE Conference on Computer Vision and Pattern Recognition. New York: IEEE, 2016: 770-778.
[7] XI Z H, HOU C Y, YUAN K P. Medical image super resolution reconstruction based on residual network [J]. *Computer Engineering and Applications*, 2019, 55(19): 191-197. (in Chinese)
[8] CHEN Y, SHI F, CHRISTODOULOU A G, et al. Efficient and accurate MRI super-resolution using a generative adversarial network and 3D multi-level densely connected network [C]// Proceedings of the Medical Image Computing and Computer Assisted Intervention. Cham: Springer, 2018: 91-99.
[9] ANKITHA B, SRIKANTH C, VENKATESH D, et al. Enhancing the resolution of brain MRI images using generative adversarial networks (GANs) [C]//International Conference on Computational Intelligence and Sustainable Engineering Solutions. New York: IEEE, 2023: 19-25.
[10] IWAMOTO Y, TAKEDA K, LI Y H, et al. Unsupervised MRI super resolution using deep external learning and guided residual dense network with multimodal image priors [J]. *IEEE Transactions on Emerging Topics in Computational Intelligence*, 2023, 7(2): 426-435.
[11] LIN J H, MIAO Q, SURAWECH C, et al. High-resolution 3D MRI with deep generative networks via novel slice-profile transformation super-resolution [J]. *IEEE Access*, 2023, 11: 95022-95036.
[12] ZHANG Y L, TIAN Y P, KONG Y, et al. Residual dense network for image super-resolution [C]//IEEE Conference on Computer Vision and Pattern Recognition. New York: IEEE, 2018: 2472-2481.
[13] LI J C, FANG F M, MEI K F, et al. Multi-scale residual network for image super-resolution [C]//Proceedings of the European Conference on Computer Vision. New York: IEEE, 2018: 517-532.
[14] CHEN N, WANG S Y, LU R, et al. Clothing parsing based on multi-scale fusion and improved self-attention mechanism [J]. *Journal of Donghua University* (*English Edition*), 2023, 40(6): 661-666.
[15] REN H, WANG X G. Review of attention mechanism [J]. *Journal of Computer Applications*, 2021, 41(S1): 1-6. (in Chinese)
[16] ZHA J H, YAN C R, ZHANG Y T, et al. Image retrieval with text manipulation by local feature modification [J]. *Journal of Donghua University* (*English Edition*), 2023, 40(4): 404-409.

基于 GAN 和多尺度密集残差注意力机制网络的磁共振图像超分辨率重建

管纯灵，禹素萍*，许武军，范　红
东华大学 信息科学与技术学院，上海 201620

摘　要：图像超分辨率重建技术在医学领域的应用有着重大意义，可以辅助医生做出更精准的诊断。然而仅使用卷积神经网络（convolutional neural network，CNN）作为生成网络，其超分辨率（super-resolution，SR）图像可能存在细节模糊和过度平滑等问题。针对这些问题，提出了基于生成对抗网络（generative adversarial network，GAN）框架的算法。在生成器中，采用由残差密集结构连接的三种不同大小卷积提取细节特征，并结合并行的通道与空间信息的注意力机制将算力集中到重要区域。在判别器中，使用 InstanceNorm 方法对图像张量进行归一化，在加快训练过程的同时保留特征信息。实验结果表明，与其他方法相比，该算法的峰值信噪比和结构相似性指数更高，视觉质量得到提高。

关键词：磁共振；图像超分辨率；注意力机制；生成对抗网络；多尺度卷积